Ab initio Simulations of Superionic H_2O, H_2O_2, and H_9O_4 Compounds

Burkhard Militzer[1,2,a)] and Shuai Zhang[1,3]

[1]*Department of Earth and Planetary Science, University of California, Berkeley, CA 94720, USA*
[2]*Department of Astronomy, University of California, Berkeley, CA 94720, USA*
[3]*Lawrence Livermore National Laboratory, Livermore, California 94550, USA*

[a)]Corresponding author: militzer@berkeley.edu

Abstract. Using density functional molecular dynamics simulations, we study the behavior of different hydrogen-oxygen compounds at megabar pressures and several thousands of degrees Kelvin where water has been predicted to occur in superionic form. When we study the close packed hcp and dhcp structures of superionic water, we find that they have comparable Gibbs free energies to the fcc structure that we predicted previously [Phys. Rev. Lett., 110 (2013) 151102]. Then we present a comprehensive comparison of different superionic water candidate structures with $P2_1$, $P2_1/c$, $P3_121$, $Pcca$, $C2/m$, and $Pa\bar{3}$ symmetry that are based on published ground-state structures. We find that the $P2_1$ and $P2_1/c$ structures transform into a different superionic structure with $P2_1/c$ symmetry, which at 4000 K has a lower Gibbs free energy than fcc for pressures higher than 22.8 ± 0.5 Mbar. This novel structure may also be obtained by distorting a hcp supercell. Finally we show that H_2O_2 and H_9O_4 structures will also assume a superionic state at elevated temperatures. Based on Gibbs free energy calculations at 5000 K, we predict that superionic water decompose into H_2O_2 and H_9O_4 at 68.7 ± 0.5 Mbar.

INTRODUCTION

Water is one of the most prevalent substances in the solar system [1]. Since it existed in solid form beyond the ice line around the early sun, it was incorporated very efficiently into the four forming giant planets. These planets thus grew much more rapidly than the terrestrial planets in our solar system and reached a critical size early enough to accret a substantial amount of gas before that was driven away by the solar wind.

Characterizing water at the condition of giant planet interiors of megabar pressure and thousands of degrees Kelvin is therefore crucial for our understanding the interior structure and evolution of these planets. Uranus and Neptune have unusual, non-dipolar magnetic fields that is assumed to be generated in the ice layer [2, 3]. Water may occur there in superionic form where the oxygen atoms are held in place like atoms in crystal while the much smaller hydrogen atoms diffuse throughout the oxygen sub-lattice like a fluid. Such a state would have a high ionic conductivity and contribute to the magnetic field generation.

While *ab initio* simulations consistently predicted water to assume a superionic state [4, 5, 6, 7, 8, 9], experimental confirmation that such a state exists has proven to be a challenge [10]. Static compression experiments in diamond anvil cells have reached pressures up to 2.1 Mbar [11, 12, 13]. Shock wave experiments [14, 15] have also reached higher pressures but they heat the sample significantly so that it melts for the highest pressures. However, dynamic ramp compression techniques [16] are expected to reach high pressures at comparatively low temperatures, where so far only theoretical methods have predicted the state of water.

Over the course of the last seven years, much theoretical effort has been put into characterizing the state of water ice at megabar pressures. Starting with Ref. [17], a series of structures have been predicted for the ground-state [18, 19, 20, 21, 22]. A H_4O stoichoimetry was predicted to become stable at 14 Mbar [22]. Soon after, Pickard *et al.* [23] predicted H_2O ice would cease to exist at approximately 50 Mbar and decompose into H_2O_2 and an hydrogen-rich structure like H_9O_4. As we will demonstrate in this article, a similar decomposition occurs in superionic water. H_2O_2 and H_9O_4 also become superionic at elevated temperatures. Our *ab initio* Gibbs free energy calculations show the decomposition of superionic H_2O is favored for pressures above 68.7 ± 0.5 Mbar.

We previously predicted a transition from a body-centered cubic (bcc) to face-centered cubic (fcc) oxygen sub-lattice in superionic water at approximately 1 Mbar [8]. In this paper, we show with *ab initio* simulations that other close packed structures have Gibbs free energies that are very similar to that of fcc and we can therefore no longer predict with certainty which close packed structure superionic water will assume up to ~22.8 ± 0.5 Mbar. Consistent with the findings in Ref. [24], we predict superionic water assume a novel structure with $P2_1/c$ symmetry that is not close packed but more dense than fcc at the same *P-T* conditions [25]. This transformation is accommodated by changes in the oxygen sub-lattice.

DENSITY FUNCTIONAL MOLECULAR DYNAMICS SIMULATIONS AND GIBBS FREE ENERGY CALCULATIONS

All *ab initio* simulations were based on density functional molecular dynamics (DFT-MD) and performed with the VASP code [26]. We used pseudopotentials of the projector-augmented wave type [27] with core radii of 1.1 and 0.8 Bohr for the O and H atoms respectively. For most calculations, we used the exchange-correlation functional of Perdew, Burke and Ernzerhof [28] but we employed the local density approximation (LDA) for comparison. A cutoff energy of 900 eV for the plane wave expansion of the wavefunctions was used throughout. The Brillioun zone was sampled with $2 \times 2 \times 2$ Monkhorst-Pack *k*-point grids [29]. $4 \times 4 \times 4$ grids had been tested [8] and yielded consistent results. The occupation of electronic states are taken to be a Fermi-Dirac distribution set at the temperature of the ions [30]. The simulation time ranged between 1.0 and 5.0 ps. A time step of 0.2 fs was used.

An initial configuration for a particular structure is obtained by starting from the ground state and gradually increasing the temperature during the DFT-MD simulation until the hydrogen atoms are mobile and equilibration is reached. Positions and velocities of equilibrated superionic structures were recycled to initialize simulations at other densities and temperatures after adjusting the cell parameters or velocities, respectively. We found that all ice structures transform into a superionic state at megabar pressures. Depending on the structure, the solid-to-superionic transition may be accompanied by re-arrangements of the oxygen sub-lattice that needs to be analyzed for every structure and density.

All simulations were performed in supercells with between 48 and 108 molecules. We used our algorithm [31] to construct compact supercells of cubic or nearly cubic shape by starting from the primitive cell vectors $\vec{a}_p$, $\vec{b}_p$, and $\vec{c}_p$:

$$\vec{a} = i_a\vec{a}_p + j_a\vec{b}_p + k_a\vec{c}_p \quad , \quad \vec{b} = i_b\vec{a}_p + j_b\vec{b}_p + k_b\vec{c}_p \quad , \quad \vec{c} = i_c\vec{a}_p + j_c\vec{b}_p + k_c\vec{c}_p \quad . \tag{1}$$

The integer values, (i_a j_a k_a, i_b j_b k_b, i_c j_c k_c), will be specified in each case.

While some structures like fcc have no adjustable cell parameters, other less symmetric crystal structures may have up to five free parameters, the b/a and c/a ratios as well as the three angles, for a given volume and temperature. Most simply one can derive these parameters with ground-state structural relaxation. Since all superionic properties are neglected in such optimizations, the results need to be confirmed with finite temperature DFT-MD simulations. If there is just one free parameter, such as the c/a ratio in the hcp structure, one can perform a series of constant-volume simulations for different c/a ratios and determine the optimal value by fitting a linear stress-strain relationship, $\sigma_{zz} - (\sigma_{xx} + \sigma_{yy} + \sigma_{zz})/3 = A(c/a) + B$, where σ_{ij} are the time-averaged components of the stress tensor. The optimal c/a ratio is given by $-B/A$ when the system is under hydrostatic conditions.

For systems with more free cell parameters, it may be more efficient to perform constant-pressure, flexible cell simulations [32]. All free parameters will then fluctuate around a mean value that can be estimated by taking a simple average. Since the fluctuations may be quite large, one can introduce a bias into the average. By monitoring the stress value during the MD simulations, one may only consider cell parameter value for the average if the instantaneous stress coincides with the target stress. Alternatively, one may use the the stress-strain pairs from the MD trajectory to fit a linear relationship $\sigma_{ij} - \sigma_{ij}^{\text{target}} = A\epsilon_{ij} + B$. The optimal strain value is again given by $-B/A$. We have tested all these three methods and found them to have comparable accuracy, which is primarily controlled by the length of the MD trajectory.

We derive the *ab initio* Gibbs free energies with a thermodynamic integration (TDI) technique [33, 34, 35, 36, 37, 38, 39, 40, 41, 42] that we adapted to superionic systems in Ref. [8]. In this scheme, the difference in Helmholtz free energy between a DFT system and a system governed by classical forces is computed from,

$$F_{\text{DFT}} - F_{\text{cl}} = \int_0^1 d\lambda \ \langle V_{\text{KS}} - V_{\text{cl}} \rangle_\lambda . \tag{2}$$

The angle brackets represent an average over trajectories governed by forces that are derived from a hybrid potential energy function, $V_\lambda = V_{cl} + \lambda(V_{KS} - V_{cl})$. V_{cl} is the potential energy of the classical system and V_{KS} is the Kohn-Sham energy. We typically perform five independent simulations with λ value equally spaced between 0 and 1.

In order to maximize the efficiency of evaluating the integral in Eq. (2), we construct a new set of classical forces for each density and temperature. Our classical reference system consists of a pair potentials between each pair of atomic species combined with a harmonic Einstein potential for every oxygen atom. The harmonic force constants are derived first from the mean square displacements in a constant-volume simulation. The residual forces are fitted to O-O, O-H, and H-H pair potentials [43] that we present with spline functions [44].

The free energy of the classical reference system, F_{cl}, is obtained with classical Monte Carlo simulations where we again take advantage of the TDI technique to gradually turn off all pair forces. The free energy of an Einstein crystal of oxygen atoms and that of a gas of noninteracting hydrogen atoms is known analytically.

COMPARISON OF DIFFERENT H_2O STRUCTURES

In Ref. [8], we predicted superionic water to assume a fcc structure at megabar pressures while earlier *ab initio* simulations had assumed a bcc oxygen sub-lattice. We begin the discussion in this section by comparing the Gibbs free energy of fcc with that of other close packed structures. In particular we will consider a hexagonal close packed (hcp) structure with an ABAB layering and double hexagonal close packed (dhcp) structure with an ABAC layering [45].
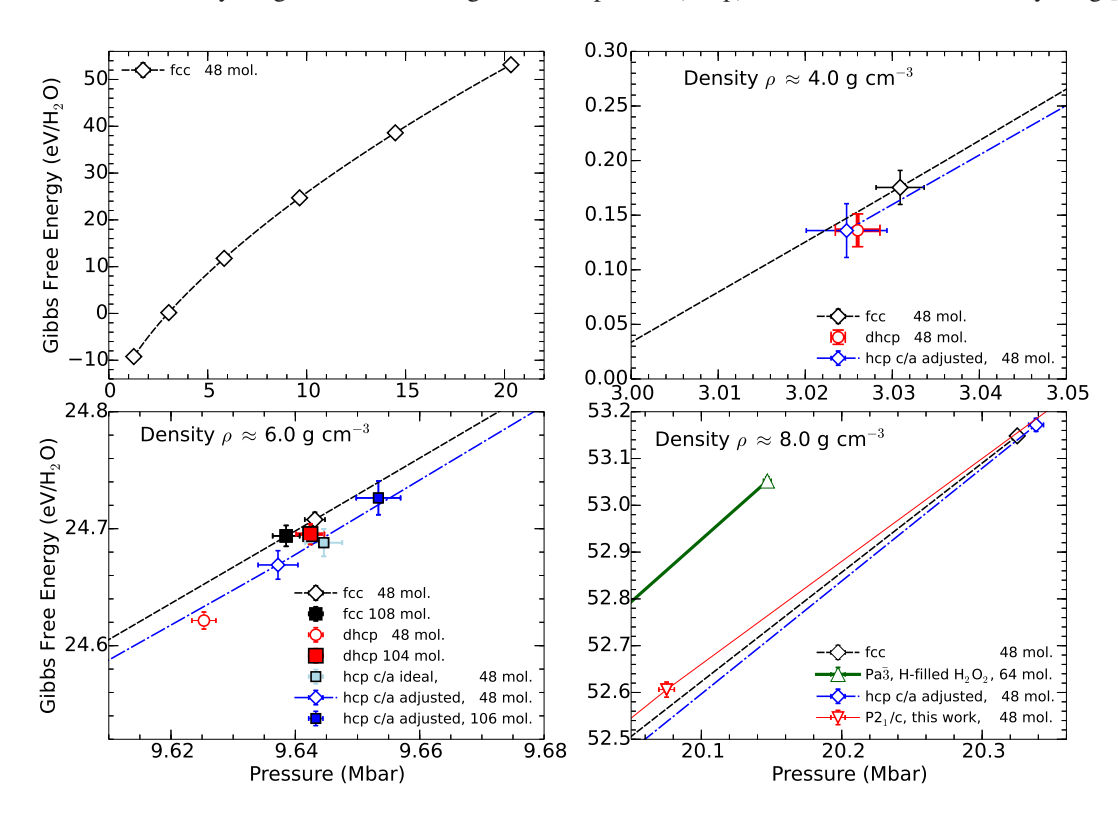

FIGURE 1. Gibbs free energy as a function of pressure at 4000 K. While the left upper shows results for the fcc structure over a large pressure range, the remaining diagrams compare different structure at a particular density. The number of H_2O molecules in the supercell is indicated in the caption.

We performed Gibbs free energy calculations for fcc, hcp, and dhcp structures for a number of densities and supercell sizes at a temperature of 4000 K. Figure 1 compares our results for 4.0, 6.0, and 8.0 $\mathrm{g\,cm}^{-3}$. When we performed calculation for dhcp at 6.0 $\mathrm{g\,cm}^{-3}$ using a (4 2 0, 0 -3 0, 0 0 -1) supercell with 48 molecules, we obtained a Gibbs free energy that was slightly below that of fcc. A further analysis revealed, however, that this deviation was caused by finite size effects. Our simulation of dhcp using a significantly larger (3 -1 1, -3 -4 0, -2 1 1) supercell with

104 molecules yielded a Gibbs free energy within the error bars of the fcc result. Conversely, fcc simulations with 48 and 108 molecules using (3 1 -1, 3 -3 -1, 0 -2 4) and cubic (3 3 -3, 3 -3 3, 3 -3 -3) supercells gave very similar Gibbs free energies. For the hcp structure, we performed simulations with 48 and 106 molecules in (4 2 0, 0 -3 0, 0 0 -2) and (4 0 1, 3 4 -1, 0 -3 -2) supercells. Again we find that the largest simulations agree with the fcc Gibbs free energy. For 4.0 and 8.0 g cm^{-3} results are also very similar. While we favored an fcc structure in our earlier publication [8], we are not able to predict with certainty which close packed structure will be realized at megabar pressures. The magnitude of the statistical and finite size uncertainties in our current Gibbs free energy calculation make the distiction between different close packed superionic structure very challenging. It is conceivable that the different structures may be realized or co-exist depending on the specific pressure, temperature, and type of hydrogen isotopes.

Hcp and dhcp structures have one free parameter that needs to be adjusted, the c/a ratio. At 4.0, 6.0, and 8.0 g cm^{-3}, we performed fixed-cell simulations of hcp and dhcp for four different c/a ratios at 4000 K. We determined an optimized c/a value from a linear fit to the stress-strain relation. For dhcp, we did not identify a significant deviation from experimental value of $1.007 \times (c/a)_{\text{ideal}}$ [45], where the ideal c/a value is given by $\sqrt{8/3}$. For hcp in the density interval from 4.0 to 8.0 g cm^{-3}, the optimized c/a ratio increased from 1.005 to 1.013 times the ideal value. However, as Fig. 1 shows, the optimization of the c/a ratio did not lead to any significant lowering of the Gibbs free energy compared to simulation with the ideal value.

After considering the close packed structures, we now focus on different ground-state structures in order to test whether any of them leads to superionic structures that are structurally stable and, more importantly, have a lower Gibbs free energy than fcc. A hexagonal structure with $P3_121$ symmetry has been proposed by Pickard *et al.* [23] to be the ground-state structure in pressure interval from 8 to 14 Mbar. We constructed a (2 2 0, 1 -1 0, 0 0 -1) supercell with 48 molecules. After the superionic regime had been reached in DFT-MD simulations with increasing temperature, we observed that the oxygen sub-lattice spontaneously re-arranged from a $P3_121$ symmetry to an fcc structure. As expected, subsequent Gibbs free energy calculations for this structure gave the same results as our fcc calculation within the statistical error bars. Since the re-arrangement occurred in simulations at 6.0 and 8.0 g cm^{-3}, we have no reason to study the $P3_121$ structure any further. In fact, this result provides additional support for the hypothesis that fcc structure is one of the most stable structure under these conditions.

For the pressure range from 14 to 19 Mbar, Pickard *et al.* [23] proposed an orthorhombic structure with *Pcca* symmetry. We performed DFT-MD simulations in (2 0 0, 0 2 0, 0 0 1) and (2 0 0, 0 3 0, 0 0 1) supercells with 48 and 72 molecules, respectively. In both cases, the oxygen sub-lattice changed spontaneously from a *Pcca* symmetry to an hcp structure during constant-volume simulations. Thus the *Pcca* structure does not need to be considered further and it confirms that hcp needs to be considered as an alternative, close-packed candidate structure.
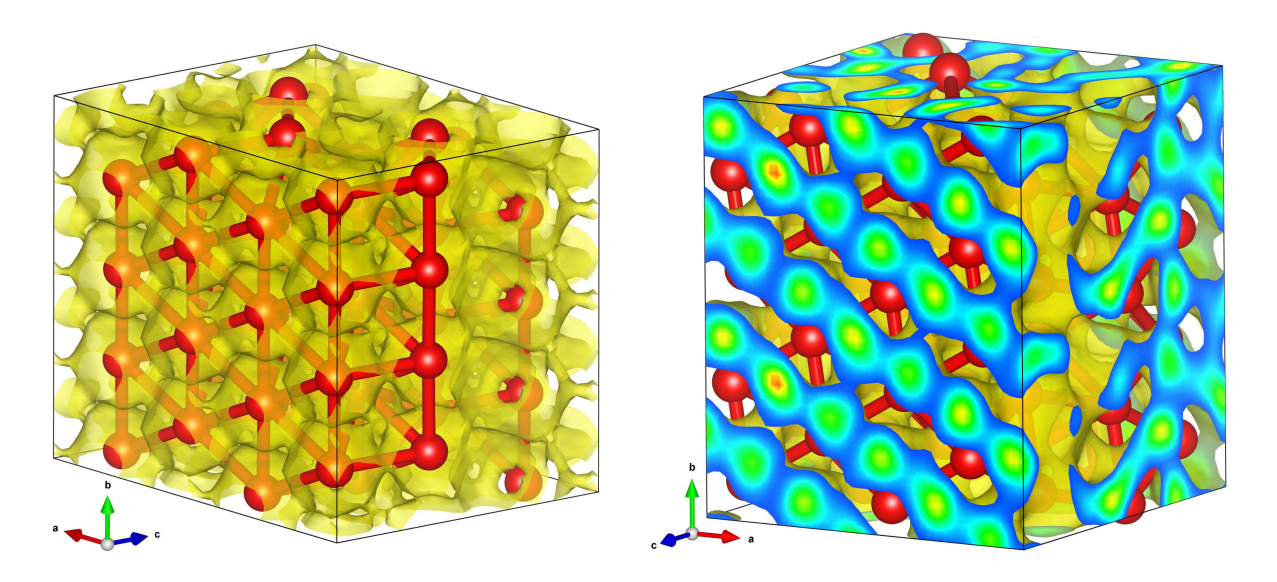

FIGURE 2. Isosurfaces of the density of hydrogen atoms are compared for hcp (left) and $P2_1/c$ (right panel). The coloring within the isosurfaces has been omitted in the upper panel for clarity. The spheres denote the oxygen atoms.

McMahon predicted that water ice assumes a metallic structure with $C2/m$ symmetry at 56 Mbar [18]. We constructed (2 -1 0, -1 -3 -1, 0 -1 2) supercells with 64 molecules and heated them to a superionic state. We determined the Gibbs free energy for densities of 11.0, 11.5, and 11.9 $g\,cm^{-3}$ but found them to be consistently higher than that of close packed structures.

TABLE 1. Lattice parameters of the monoclinic primitive cell derived from simulations of our $P2_1/c$ structure at different densities and temperatures. The last three columns specify the fractional coordinates of the oxygen atom in Wyckoff position e with multiplicity 4. † labels cell parameters that we obtained by extrapolation in pressure before the oxygen positions were obtained by averaging over MD trajectories.

T (K)	P (Mbar)	ρ $(g\,cm^{-3})$	a (Å)	b (Å)	c (Å)	β(°)	x	y	z
5000	74.88	13.89	2.380	2.542	2.946	28.91	0.3516	0.3653	-0.08432
5000	69.87	13.47	2.404	2.571	2.976	28.88	0.3538	0.3644	-0.08483
5000	59.92	12.59	2.458	2.633	3.050	28.78	0.3486	0.3638	-0.08094
5000	49.91	11.63	2.523	2.709	3.132	28.73	0.3460	0.3638	-0.07871
5000	39.91	10.57	2.608	2.801	3.240	28.58	0.3417	0.3640	-0.07602
4000	27.13	9.040	2.743	2.959	3.411	28.56	0.3384	0.3638	-0.07367
4000	23.54	8.529	2.802	3.011	3.467	28.66	0.3293	0.3602	-0.06637
4000	17.13	7.503	$2.921^{\dagger}$	$3.151^{\dagger}$	$3.627^{\dagger}$	$28.53^{\dagger}$	0.3086	0.3574	-0.04738

This leaves us with two more structures to consider. Before the work by Pickard *et al.* [23], a monoclinic structure with $P2_1$ symmetry had been proposed by several authors [18, 19, 20, 21] for the pressure interval from 11.7 to 19.6 Mbar. We performed superionic DFT-MD simulations in (3 0 0, 0 2 0, 0 0 2) and (3 1 0, -2 2 0, -1 0 -2) supercells with 48 and 64 molecules, respectively. We found that the oxygen sub-lattice re-arranges to a new monoclinic structure with $P2_1/c$ symmetry with just four oxygen atoms per unit cell. Table 1 provides the structural parameters for different conditions. The cell parameters were determined first with constant-pressure simulations. The oxygen position derived by averaging over trajectories obtained in subsequent constant-volume simulations. Below 20 Mbar, the $P2_1/c$ structure exhibited an instability in constant-pressure simulations. Since we need cell parameters for Gibbs free energy calculations under these conditions, we extrapolated the cell parameters that we obtained from simulation at higher pressure.

Before we analyze the properties of our $P2_1/c$ structure in more detail, we discuss the monoclinic $P2_1/c$ structure with eight molecules per unit cell that was predicted by Ji *et al.* [19] to be the ground state in the pressure range from 19.6 to 50 Mbar. We constructed a triclinic (2 0 1, 0 2 1, 0 -1 1) and a monoclinic (2 0 1, 0 2 0, 0 0 -2) supercell with 48 and 64 molecules, respectively. When the simulations reached a superionic state, the oxygen sub-lattice re-arranged itself to the same $P2_1/c$ structure that we had obtained earlier by heating the $P2_1$ supercells. The resulting structural parameters were indistinguishable from those in Tab. 1.

When we analyzed the average density of hydrogen atoms in Fig. 2, we found it to be very non-uniform. This distinguishes the $P2_1/c$ phase from close packed superionic structures. This finding is consistent with diffusion rates being anisotropic in this structure [24].

We also lowered the pressure step by step in our constant-pressure flexible-cell simulations of the $P2_1/c$ structure in order to identify a transformation path to a close packed structure. At 14, 17, and 20 Mbar, the $P2_1/c$ structure transformed into a nearly perfect hcp structure as is illustrated in Fig. 4. The relaxation to a perfect hcp crystal is prevented by our choice of supercell. This becomes apparent when the stacking of layers is viewed along the b direction. Nevertheless, the resulting structure is sufficiently close to hcp so that we can propose a transformation path the we illustrate in Fig. 4. The hcp-to-$P2_1/c$ transformation appears to be facilitated by a shift of the a-b planes. While a view of the hcp structure along the c direction reveals perfect hexagons as a results of the ABAB layering, these hexagons appear distorted in the $P2_1/c$ crystal as a result of the layer shift. In our experience, these distorted hexagons provide the most straightforward way to identify the $P2_1/c$ structure. While in hcp, or any other close packed system, every atom has twelve equally-distant nearest neighbors. In the $P2_1/c$ crystal, the distortion groups the oxygen atoms into pairs. For a crystal at a density of 9.8 $g\,cm^{-3}$, this implies every oxygen atom has one nearest neighbor that is 1.45 Å away and two next-neighest neighbors at 1.49 Å. There are five atoms at distances betwee 1.52 and 1.56 Å. The remaining four neighbors are between 1.70 and 1.73 Å away.

We performed two sets of Gibbs free energy calculations for the $P2_1/c$ structure: one using the cell parameters derived from ground-state relaxation, and the other refined with constant-pressure MD simulations. Figure 3 compares the resulting Gibbs free energies with those from a fcc crystal. Both sets of $P2_1/c$ calculations demonstrate clearly
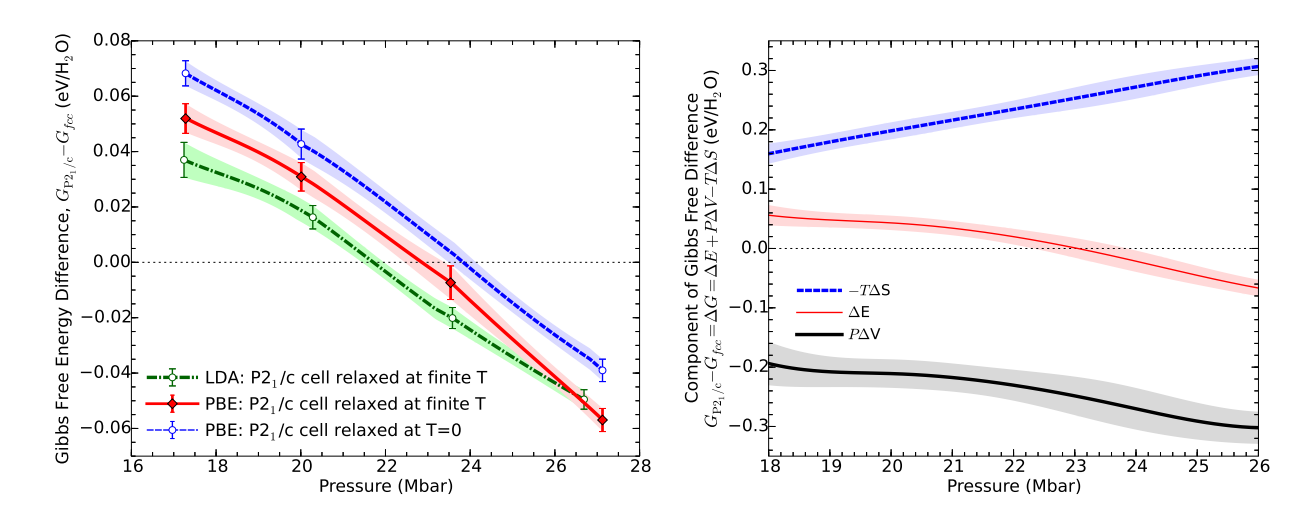
FIGURE 3. Gibbs free energy difference between the $P2_1/c$ and fcc structures at 4000 K. On the left, the red and the blue curves correspond to two calculations of the total Gibbs free energy difference using the PBE functional. For the blue curve, the $P2_1/c$ lattice parameters were taken from ground-state calculations, while for the red curve, they have been optimized with constant-pressure simulations. Based on the latter, more accurate determination, the transition from the fcc to $P2_1/c$ structure predicted to occur at 22.8 ± 0.5 Mbar. From comparison, a calculation with the LDA functional yields lower transition pressure of 21.7 ± 0.3 Mbar (green curve).The shaded regions indicate the statistical uncertainties. On the right, various components of the Gibbs free energy difference are displayed.

that there is a transition from fcc to $P2_1/c$. The lattice parameter refinement lowers the Gibbs free energy of the $P2_1/c$ structure slightly, which lowers the transition pressure by about 1 Mbar to a value of 22.8 ± 0.5 Mbar, which we consider our most accurate prediction for the transition pressure from fcc to the $P2_1/c$ structure. To obtain an estimate how sensitive this prediction depends on the exchange-correlation functional, we we recomputed the Gibbs free energy between the $P2_1/c$ and fcc structures within the LDA. We obtained a slightly lower transition pressure of 21.7 ± 0.3 Mbar. The magnitude of this difference is not unexpected because LDA typically predicts higher densities and lower transition pressures [46] than are obtained with experiments and DFT calculations with other functionals. This was in fact one of the original motivations for developing the PBE functional [28].

Figure 3 also shows the Gibbs free energy difference between fcc and $P2_1/c$ split up into its three components. The $P\Delta V$ term is negative and confirms that the $P2_1/c$ structure is more dense than fcc at the same pressure and temperature. Since fcc is a close packed structure as far as the oxygen sub-lattice is concerned, this density change must be accommodated by the hydrogen atoms or by changes in the electronic structure. $-T\Delta S$ term suggests that significant changes occur in the hydrogen sub-system. This term is positive and thus counteracts a transformation to $P2_1/c$. It also reflects a reduction in the mobility of the hydrogen atoms, which is consistent with the non-uniform density of hydrogen atoms shown in Fig. 2. We consider this change to a less uniform hydrogen sub-system to be the primary reason for a change from a close packed superionic system to the $P2_1/c$ structure.

The difference in internal energy in Fig. 3 is small compared to the other Gibbs free constituents but it decreases with pressure and contributes to the energy balance that lead to a transition pressure of 22.8 Mbar at 4000 K.

DECOMPOSITION OF WATER INTO SUPERIONIC H_2O_2 AND H_9O_4

With a ground-state random structure search, Pickard *et al.* [23] predicted water ice to decompose into H_2O_2 and a hydrogen-rich structure like H_9O_4 at approximately 50 Mbar. Since this exceeds the density range that we have discussed so far, we now report simulation results from $10 - 13.5$ g cm^{-3}. We performed DFT-MD simulations of H_2O_2 at constant-volume in a cubic (2 0 0, 0 2 0, 0 0 2) supercell with 32 formula units. We started from the ground-state geometry at a density of 13.3 g cm^{-3}, which corresponds to a pressure of 50 Mbar, and gradually increased the temperature during the MD simulation. At a temperature of 4300 K the hydrogen atoms become mobile while the oxygen atoms remained confined to their lattice sites and the system assumed a superionic state (Fig. 6). This transition temperature is confirmed by subsequent cooling simulations that showed the system spontaneously transforming back
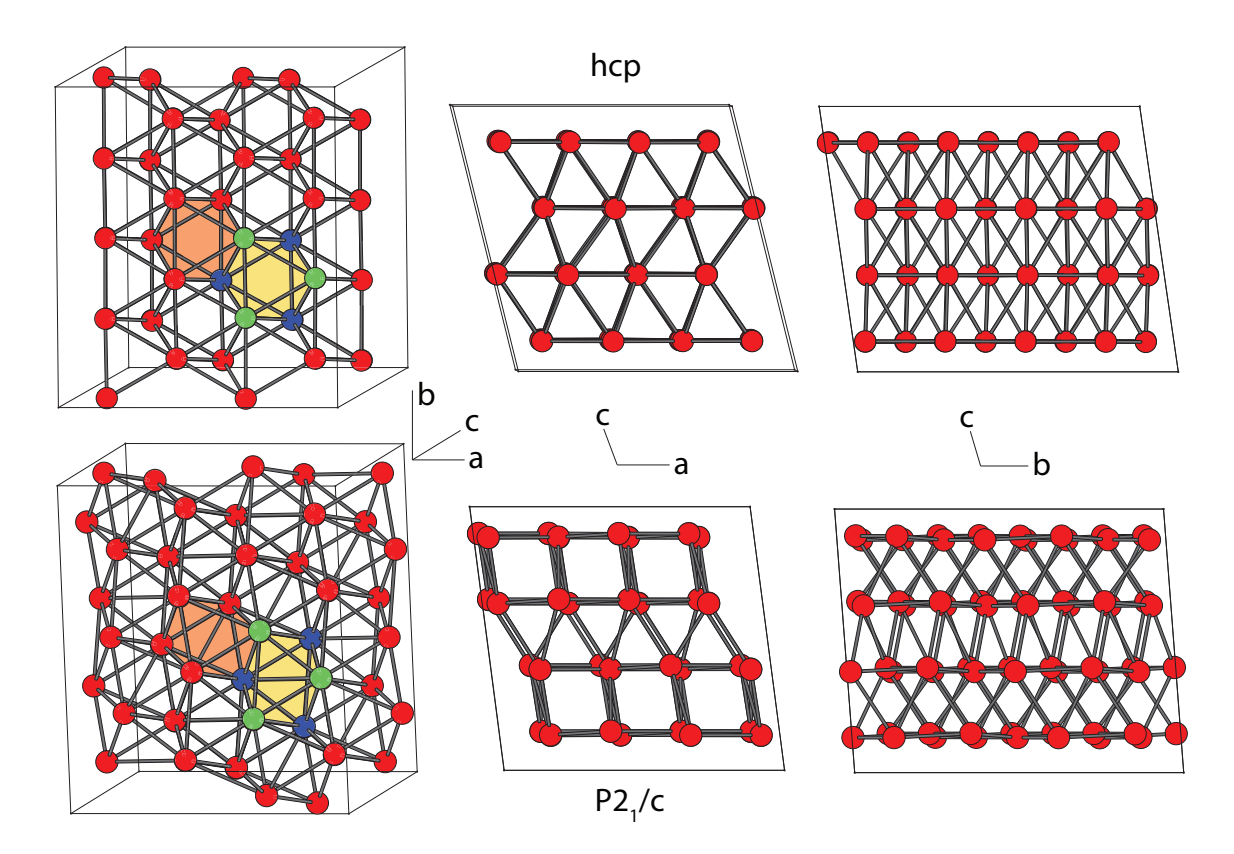
FIGURE 4. Comparison of the hcp (upper row) and novel $P2_1/c$ (lower row) structures. The spheres denote the positions of the 64 oxygen atoms in the supercell that were derived by averaging over entire MD trajectories. The lattice vectors of the supercell are shown schematically. On the left, two hexagons are shaded and three atoms in the first and second layers are colored differently in order to illustrate the hcp-to-$P2_1/c$ transformation that is facilitated by the sliding of a-b planes. While the diagram in the upper center shows the characteristic hexagonal pattern of a close packed structure, the corresponding diagram in the lower center shows stacked layers composed of nearly perfect squares and triangles for $P2_1/c$. On the right, the view along the b direction also illustrates modest differences.

to a solid state.

The oxygen sub-lattice appears to be significantly more stable than in close-packed simulations at comparable conditions. In H_2O_2 simulations at 13.3 g cm^{-3}, 51.9 Mbar, and 6000 K, the root mean squared displacement of the oxygen atoms from their $Pa\bar{3}$ lattice sites was only 0.14 Å while in simulations of fcc H_2O at comparable P-T conditions was approximately 0.21 Å. This observation prompted us to perform a number of additional investigations. First we filled the superionic structure step by step with additional hydrogen atoms. We were able to reach a H_2O stoichiometry while maintaining a stable superionic structure. Any further addition of hydrogen atom destabilized the $Pa\bar{3}$ oxygen sub-lattice, however. We performed Gibbs free energy calculations of this superionic H_2O structure at 5, 6, 8, 10 and 11 g cm^{-3}. Even though this structure exhibits a density 0.5% higher than that of close-packed structures at same pressure, its Gibbs free energy was always significantly higher (Fig. 1). We therefore concluded the superionic water with a $Pa\bar{3}$ oxygen sub-lattice is not thermodynamically stable.

Since the $Pa\bar{3}$ oxygen sub-lattice exhibits such an efficient packing, we also investigated whether it would lead to H_2O groundstate structures that are more stable than existing predictions [18, 19, 20, 21, 23]. We thus performed a ground-state random structure search for favorable hydrogen positions in the H_2O stoichiometry while starting from a $Pa\bar{3}$ oxygen sub-lattice each time. As most stable, we identified another structure with $P2_1/c$ symmetry that differed from that of Ji *et al.*[19]. Still, this $P2_1/c$ structure has a higher enthalpy than other proposed ground-state structures for all densities under consideration. Therefore, we did not study hydrogen-filled $Pa\bar{3}$ oxygen sub-lattices any further.

For simulations of superionic H_9O_4, we constructed (2 1 -1, -2 2 1, -2 0 -1) supercells with 156 atoms (12 formula units) starting from the the ground-state geometries [23]. This supercell was chosen to be comparable in size
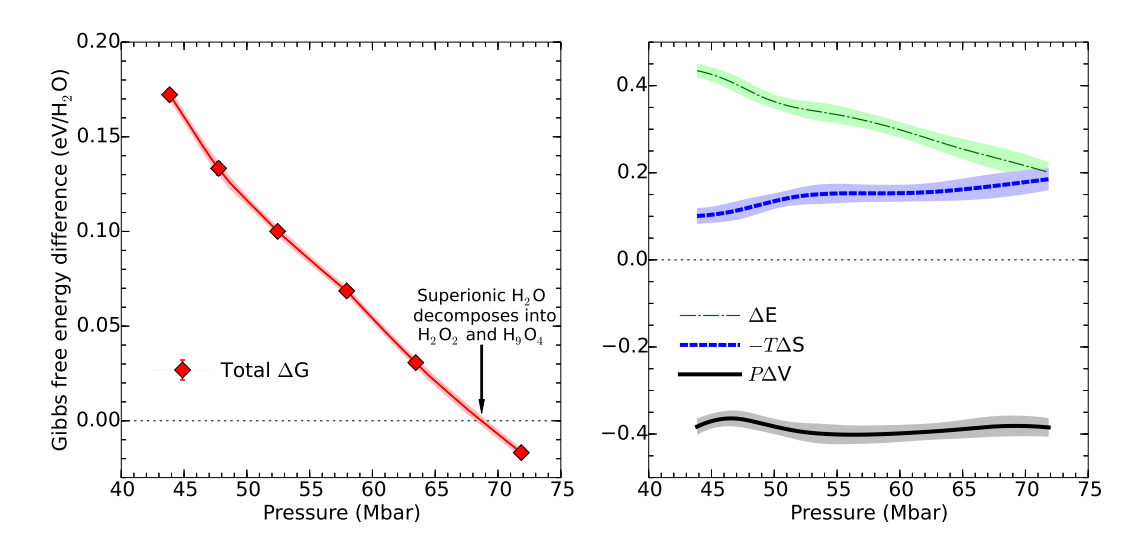
FIGURE 5. Gibbs free energy difference, $\Delta G(\text{eV}/H_2O) = [G(H_2O_2) + 2G(H_9O_4)]/10 - G(H_2O)$, for 5000 K as a function of pressure. The change of sign on the upper panel demonstrates the H_2O decomposes into H_2O_2 and H_9O_4 at the a pressure of 68.7 ± 0.5 Mbar. The right panel shows the different components on the Gibbs free energy difference.

to our other simulations. During our heating simulations, the H_9O_4 system assumed a superionic state (Fig. 6) at a temperature of approximately 1600 K.

We performed Gibbs free energy calculations for H_2O, H_2O_2, and H_9O_4 structures at 5000 K for a series of densities in order to cover the pressure interval from 45 to 70 Mbar. To demonstrate that H_2O decomposes into H_2O_2 and H_9O_4, we need to show that there is a sign change in Gibbs free energy difference per H_2O formula unit,

$$\Delta G = [\, G(H_2O_2) + 2\, G(H_9O_4)\,]/10 - G(H_2O)\,. \tag{3}$$

Figure 5 shows that such a sign change indeed occurs at a pressure of 68.7 ± 0.5 Mbar implying that superionic H_2O decomposed into a heterogeneous mixture of superionic H_2O_2,and H_9O_4 at this pressure. In the lower panel of Fig. 5, we have separated the Gibbs free energy difference into its different components. The $P\Delta V$ term is consistently large and negative, implying that the decomposition of superionic H_2O is primarily triggered by a more efficient packing in the H_2O_2 and H_9O_4 crystal structures. Consistent with this argument, we find that sign of the $-T\Delta S$ term is positive, implying the hydrogen atoms appear to have slightly more space to move around in the H_2O structure. The ΔE term is positive and favors an H_2O stoichiometry but it decays with increasing pressure. This trend eventually changes the sign of the Gibbs free energy balance, which leads to the decomposition of H_2O at 68.7 ± 0.5 Mbar. This prediction is at variance with the recent work by French *et al.* [47] who suggested that the fcc superionic phase transforms back to bcc at 50±10 Mbar at 5000 K. In their work, only bcc and fcc phases were considered and the entropy was derived from the vibrational density of states (VDOS). As stated in Ref. [47], this method is less accurate than the TDI technique that we employed here for the following reasons. There are different contributions to the entropy of many-body systems that need to treated separately. French *et al.* employ a two-phase model to split the VDOS in gas-like and solid-like parts. This splitting and the treatment of each term rely to some degree on approximations. In comparison, the TDI technique is simpler. As long as Eq. 2 is evaluated with sufficient accuracy, all nuclear and electronic contributions to the entropy are included [38]. The VDOS approach does, however, allow one to include nuclear quantum effects, which we do not consider here.

Using the TDI approach, we determined a decomposition pressure of 68.7 ± 0.5 Mbar for superionic water that is higher than the 50 Mbar that was predicted for the decomposition of solid H_2O ice at zero temperature [23]. Such a pressure shift is not unexpected since we are dealing with different oxygen sub-lattices and, more importantly, an entropy term, $-T\Delta S$, which is only relevant at finite temperature. This term is positive and approximately 0.1 eV/H_2O. Fig. 5 shows that such a Gibbs free energy change shift the transition pressure by +16 Mbar. This lets us conclude that the entropy associated with the hydrogen motion is the primary reason why our decomposition pressure for superionic water is higher that for water ice.
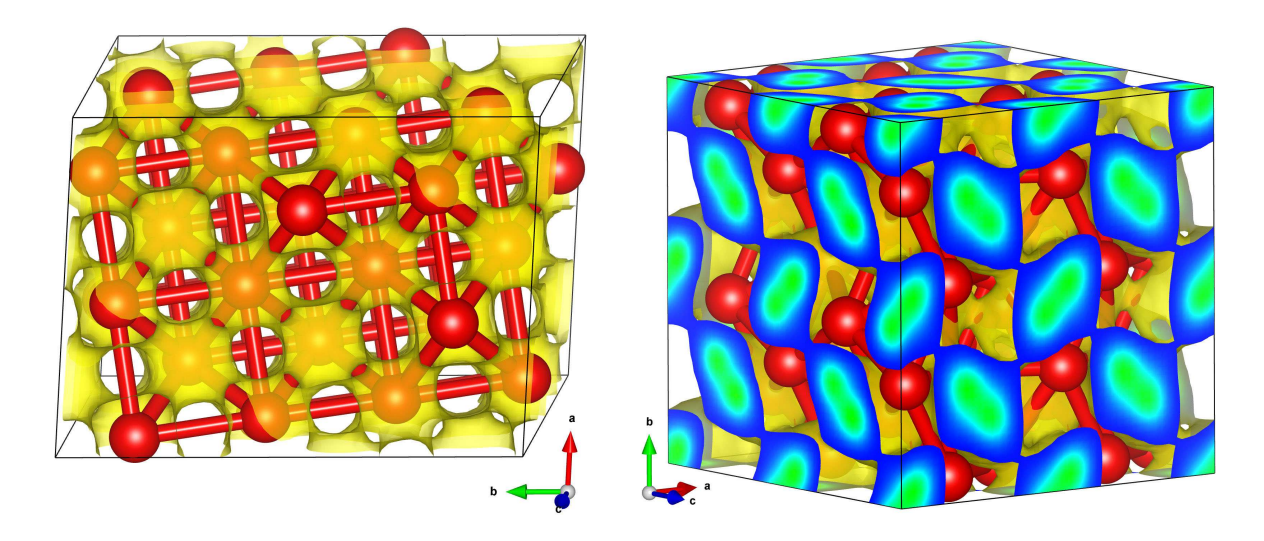
FIGURE 6. Isosurfaces of the density of hydrogen atoms are compared for H_9O_4 (left) and H_2O_2 (right).

CONCLUSIONS

We have presented more information about the phase diagram of water at megabar pressures by performing *ab initio* simulations of superionic water for a series of candidate structures. We showed that the several close packed structures, fcc, hcp, and dhcp, have very similar Gibbs free energies. The differences are on the order of ~0.02 eV/H_2O. Given the statistical and finite size uncertainties of our current Gibbs free energy calculations, we are not able to predict with certainty which superionic structure will be assumed in the pressure interval from approximately 1.0 to 23 Mbar. It is possible, however, that several stable phases may be realized or possibly co-exist depending on pressure, temperature, and types of the hydrogen isotope. For higher pressures, we find superionic water to transform into novel structure with $P2_1/c$ symmetry, in which hydrogen motion is more restricted. This structure may be obtained through a distortion of an hcp crystal.

At a much higher pressure of 68.7 ± 0.5 Mbar and temperature of 5000 K, we predict superionic water to decompose into superionic H_2O_2 and superionic H_9O_4 structures. While an analysis of the temperature dependence of this transition is beyond the scope of this work, the predicted decomposition is consistent with the decomposition that was proposed for water ice at 50 Mbar but the superionic transition pressure is a bit higher because of the entropic contribution from the hydrogen atoms to the Gibbs free energy balance.

ACKNOWLEDGMENTS

REFERENCES

[1]   W. B. Hubbard, *Planetary Interiors* (University of Arizona Press, Tucson, AZ, 1984).
[2]   N. F. Ness, M. H. Acuna, K. W. Behannon, L. F. Burlaga, J. E. P. Connery, R. P. Lepping, and F. M. Neubauer, Science **233**, 85 (1986).
[3]   S. Stanley and J. Bloxham, Nature **428**, 151 (2004).
[4]   C. Cavazzoni, G. L. Chiarotti, S. Scandolo, E. Tosatti, M. Bernasconi, and M. Parrinello, Nature **283**, 44 (1999).
[5]   N. Goldman, L. E. Fried, I.-. W. Kuo, and C. J. Mundy, Phys. Rev. Lett. **94**, 217801 (2005).
[6]   T. R. Mattsson and M. P. Desjarlais, Phys. Rev. Lett. **97**, 017801 (2006).

[7]   M. French, T. R. Mattsson, N. Nettelmann, and R. Redmer, Phys. Rev. B **79**, 054107 (2009).
[8]   H. F. Wilson, M. L. Wong, and B. Militzer, Phys. Rev. Lett. **110**, 151102 (2013).
[9]   J.-A. Hernandez and R. Caracas, Phys. Rev. Lett. **117**, 135503 (2016).
[10] A. F. Goncharov *et al.*, *J. Chem. Phys.* **130**, 124514 (2009).
[11] R. J. Hemley *et al.*, *Nature* **330**, 737 (1987).
[12] A. F. Goncharov *et al.*, *Science* **273**, 218 (1996).
[13] P. Loubeyre, R. LeToullec, E. Wolanin, M. Han, and D. Hausermann, Nature **397**, 503 (1999).
[14] K. K. M. Lee *et al. J. Chem. Phys.* **125**, 014701 (2006).
[15] M. D. Knudson, M. P. Desjarlais, R. W. Lemke, T. R. Mattsson, M. French, N. Nettelmann, and R. Redmer, Phys. Rev. Lett. **108**, 091102 (2012).
[16] J. Wang *et al.*, J. Appl. Phys. **114**, 023513 (2013).
[17] B. Militzer and H. F. Wilson, Phys. Rev. Lett. **105**, 195701 (2010).
[18] J. F. McMahon, Phys. Rev. B **84**, 220104(R) (2011).
[19] M. Ji, K. Umemoto, C.-Z. Wang, K.-M. Ho, and R. M.Wentzcovitch, Phys. Rev. B **84**, 220105(R) (2011).
[20] Y. Wang, H. Liu, J. Lv, L. Zhu, H. Wang, and Y. Ma, Nature Comm. **2**, 563 (2011).
[21] A. Hermann, N. W. Ashcroft, and R. Hoffmann, Proc. Nat. Acad. Sci. **109**, 745 (2011).
[22] S. Zhang, H. F. Wilson, K. P. Driver, and B. Militzer, Phys. Rev. B **87**, 024112 (2013).
[23] C. J. Pickard, M. Martinez-Canales, and R. J. Needs, Phys. Rev. Lett. **110**, 245701 (2013).
[24] J. Sun, B. K. Clark, S. Torquato, and R. Car, Nature Commun. **6**, 8156 (2015).
[25] In the same session of American Physical Society meeting in March 2014 where we presented the majority of the results from this work, J. Sun, B. Clark, and R. Car also predicted a phase transition in superionic H_2O water based on spontaneous transitions in constant pressure simulations of $P2_1$ supercells.
[26] G. Kresse and J. Hafner, Phys. Rev. B 47, 558 (1993); G. Kresse and J. Hafner, Phys. Rev. B 49, 14251 (1994); G. Kresse and J. Furthmüller, Comput. Mat. Sci. 6, 15 (1996); G. Kresse and J. Furthmüller, Phys. Rev. B 54, 11169 (1996).
[27] P. E. Blöchl, Phys. Rev. B **50**, 17953 (1994).
[28] J. P. Perdew, K. Burke, and M. Ernzerhof, Phys. Rev. Lett. **77**, 3865 (1996).
[29] H. Monkhorst and J. Pack, Phys. Rev. B. **13**, 5188 (1976).
[30] N. D. Mermin, Phys. Rev. **137**, A1441 (1965).
[31] B. Militzer, J. High Energy Density Phys. **21**, 8 (2016).
[32] E. Hernandez, J. Chem. Phys. **115**, 10282 (2001).
[33] G. A. de Wijs, G. Kresse, and M. J. Gillan, Phys. Rev. B **57**, 8223 (1998).
[34] M. A. Morales, C. Pierleoni, E. Schwegler, and D. M. Ceperley, Proc. Nat. Acad. Sci. **106**, 1324 (2009).
[35] H. F. Wilson and B. Militzer, Phys. Rev. Lett. **104**, 121101 (2010).
[36] H. F. Wilson and B. Militzer, Astrophys. J. **745**, 54 (2012).
[37] H. F. Wilson and B. Militzer, Phys. Rev. Lett. **108**, 111101 (2012).
[38] B. Militzer, Phys. Rev. B **87**, 014202 (2013).
[39] S. M. Wahl, H. F. Wilson, and B. Militzer, Astrophys. J. **773**, 95 (2013).
[40] F. Gonzalez-Cataldo, H. F. Wilson, and B. Militzer, Astrophys. J. **787**, 79 (2014).
[41] F. Soubiran and B. Militzer, Astrophysical J. **806**, 228 (2015).
[42] F. Soubiran and B. Militzer, Astrophysical J. **829**, 14 (2016).
[43] S. Izvekov, M. Parrinello, C. J. Burnham, and G. A. Voth, J. Chem. Phys. **120**, 10896 (2003).
[44] S. Wahl and B. Militzer, Earth and Planetary Science Letters **410**, 25 (2015).
[45] Y. Ma, A. R. Oganov, and Y. Xie, Phys. Rev. B **78**, 014102 (2008).
[46] K. P. Driver, R. E. Cohen, Z. Wu, B. Militzer, P. L. Rios, M. D. Towler, R. J. Needs, and J. W. Wilkins, Proc. Nat. Acad. Sci. **107**, 9519 (2010).
[47] M. French, M. P. Desjarlais, and R. Redmer, Phys. Rev. E **93**, 022140 (2016).